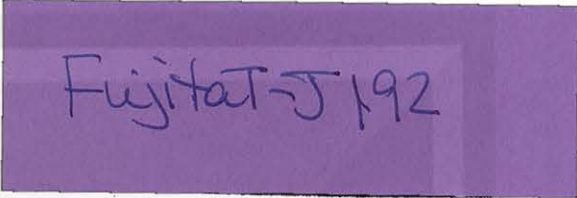


AN OVERVIEW OF MESOSCALE PREDICTION

T. Theodore Fujita

The University of Chicago
Chicago, Illinois



1. INTRODUCTION

The history of recognizing mesoscale phenomena goes back some 40 years to 1951 when the late Myron Ligda¹ pointed out the scale too large to be observed from a single station, yet too small to appear on a sectional synoptic map. He stated that phenomena of this size might well be designated as "mesometeorological." Ligda's suggestion was initiated by his research on radar echoes at Texas A and M.

On the other side of the Pacific Ocean, Fujita, isolated in the post-war years, worked on his own "microanalysis" of weather phenomena in 1947 through 1951, making use of surface-station observations, the only data available in Japan at that time. He conducted microanalysis by developing a time-space conversion technique which turned out to be very useful in depicting the spatial extent of subsynoptic phenomena.

After coming to the University of Chicago in 1953, Fujita collaborated with Morris Tepper of the U.S. Weather Bureau, formally promoting the importance of the "mesoscale" in predicting severe local storms. Upon publishing MESOANALYSIS: An Important Scale in the Analysis of Weather Data by Fujita, Newstein, and Tepper in January 1956², the analytical phase of mesometeorology was born.

Presented in this paper is an overview of mesoscale prediction which underwent low-tech to high-tech transition during the past 40 years. Needless to say, both modern radars and advanced satellites became the standard tools in collecting mesometeorological data being used for improving mesoscale predictions.

2. MESOSCALE DISTURBANCES

By virtue of their small dimensions, mesoscale disturbances are characterized by extremely large values of meteorological parameters such as energy density, rainfall rate, wind speed, pressure, temperature and humidity gradients. These values are often 10 to 100 times larger than those expected in ordinary synoptic disturbances. Mesoscale disturbances and storms accompanied by these high-value parameters are listed below.

- Thunderstorms: airmass, frontal, orographic

Footnote 1. Ligda, M. G. H. (1951) Radar storm observation. Compendium of meteorology, Boston, Amer. Meteor. Soc., 1265-1282.

Footnote 2. Fujita, T., H. Newstein, and M. Tepper (1956) MESOANALYSIS: An important scale in the analysis of weather data. U.S. Wea. Bur. Res. Paper 39, 83 pp.

- Mesocyclones: with hooks, clear-air, anticyclonic, wake depression
- Tornadoes: landspout, waterspout, gustnado
- Downbursts: macroburst, microburst, gust front
- Katabatic winds: from glacier, from canyon
- Downslope winds: Foehn, Chinook, Oroshi-kaze
- Local fog, duststorm, smoke plume
- Pressure-jump line
- Lake-effect snow: snowband, blizzard
- Temperature front: induced by local storm, urban heat island, lake and sea breeze
- Moisture front: dry front

Some of these disturbances are very local while others are seasonal. Each one, nevertheless, will require various degrees of prediction with one minute to several hours of lead time. There are numerous papers dealing with both successful and unsuccessful attempts to meet individual requirements.

3. TIME-SPACE CONVERSION METHOD

The first time-space conversion by the author was made by locating azimuth and distance of 33 lightnings

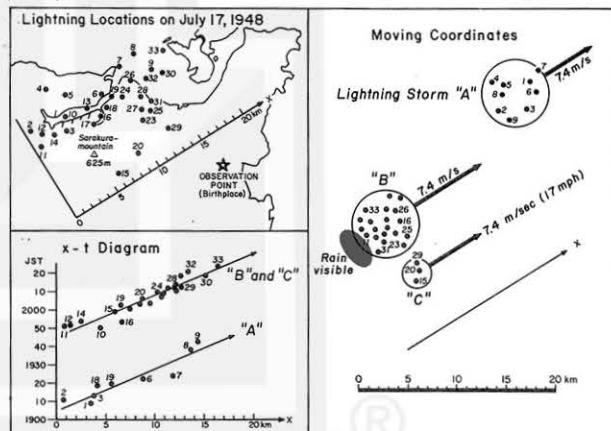


Fig. 1 Three cells of lightning storms on 17 July 1948 obtained by the time-space conversion technique. From Fujita (1951) Microanalytical study of cold front. Geophys. Mag. Japan, 22, 237-277.

determined by the flash-to-sound time of each lightning. They were first plotted on the x-t diagram (Fig. 1) for determining the traveling speed. Lightning locations were replotted on the Lagrangian coordinates moving with the storm. This conversion method finally depicted

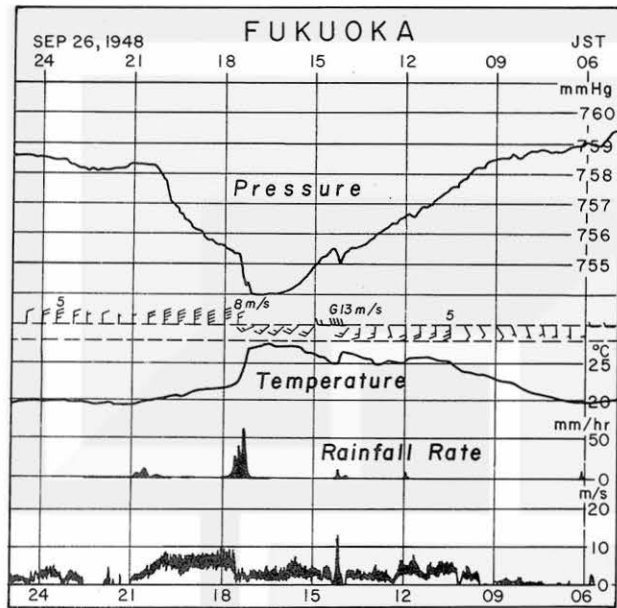


Fig. 2 Time variation of meteorological parameters from Fukuoka, Japan. One of the 45 station data from western Japan. Same reference of Fig. 1.

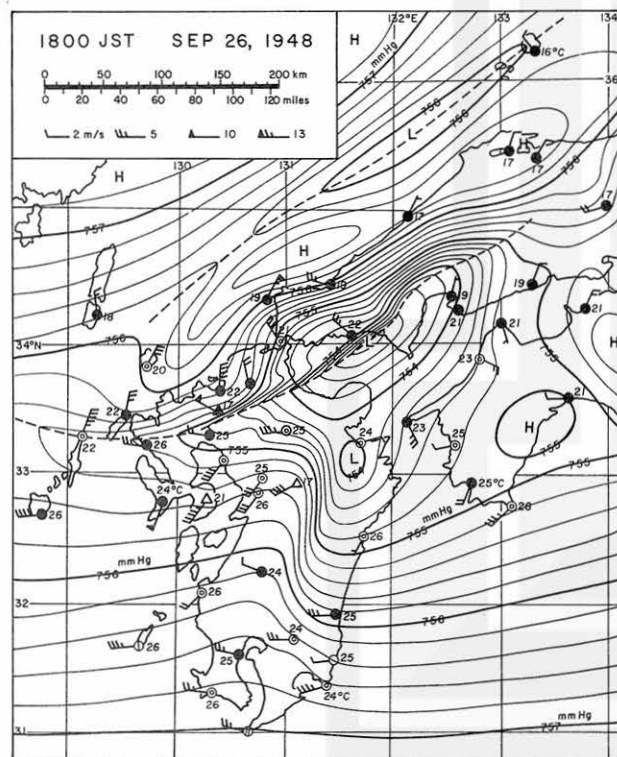


Fig. 3 The first mesoanalysis (microanalysis) map by Fujita. Presented at the Western Japan Meeting of Meteorological Society of Japan in 1949.

two major cells "A" and "B" and a minor cell "C," revealing that lightning locations were rather concentrated when viewed on moving coordinates.

The next attempt of the time-space conversion was made by collecting standard meteorological data from 45 stations in western Japan. The time section from Fukuoka (Fig. 2) for example, consists of pressure and temperature traces, rainfall rate, and winds. Because the system movement was from west-northwest, the time on the chart was increased from right to left.

The first microanalysis (mesoanalysis) chart was obtained by drawing isobars at 0.2 mmHg intervals to satisfy both pressure value and space variation of pressure at each station. In drawing isobars, unless the space-domain change in pressure is satisfied (Fig. 3), the pressure field would have been smoothed, thus washing out the mesoscale pressure fields of the squall line.

While at the University of Chicago from 1953 to 1955, the author applied his microanalysis method to the pressure-jump network data being collected by the Severe Storms Research Unit of the U.S. Weather Bureau headed by Morris Tepper. Although the average distance of the pressure-jump network stations (Fig. 4) was 160 km, 2.5 times larger than that of the Japanese stations (Fig. 3), it was rather easy to depict mesoscale highs and lows, mesohighs and mesolows, over the Midwest. As in this example, a small mesohigh in Colorado was very similar to the very early stage of the huge mesohigh centered on the Kansas-Nebraska stateline.

After completing the MESOANALYSIS paper in color, we felt equally that future mesoscale prediction will be improved tremendously if, someday, hourly mesomaps covering the entire United States become available to forecasters. Unfortunately, the density of observation stations became progressively sparse since the 1950s. On the other hand, radar and satellite data were added, allowing us to modernize the mesoanalysis maps for use by the new-generation forecasters of the 1990s.

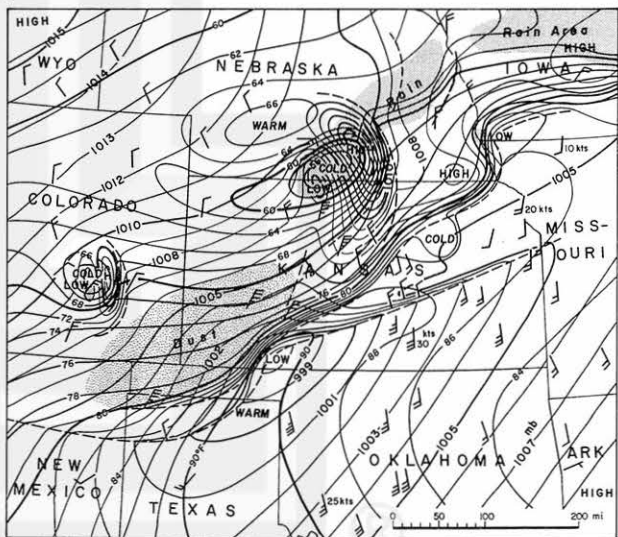


Fig. 4 One of the 10 mesoanalysis maps printed in 5 colors. From Fujita, Newstein, and Tepper (1956) MESOANALYSIS: An important scale in the analysis of weather data. (Footnote 2)

Separation of mesoscale disturbances from the undisturbed pressure field was undertaken in determining the spatial distribution of the perturbation pressure field. A number of case studies revealed that both positive and negative excess pressures often coexist inside the disturbance boundary defined as the line of zero excess pressure (Fig. 5).

It has been known that the shape and magnitude of the excess pressure field vary with the radar-echo activities, resulting in the amalgamation of a number of mesohighs. Quite often, a traveling positive (excess) pressure is followed by a negative (excess) pressure, forming a couplet of positive-negative pressure disturbances. In general, the negative pressure forms several hours after the positive-pressure formation, and the former outlives the latter. The area of the negative pressure, remaining until the next day, could induce a mesoscale convergence field, giving rise to the formation of afternoon thunderstorms.

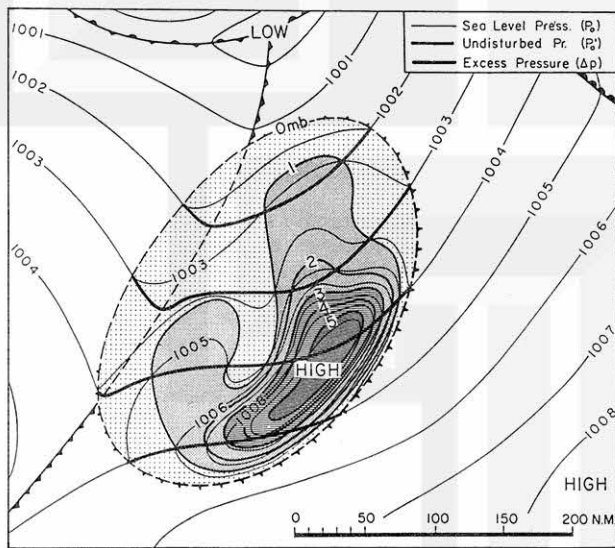


Fig. 5 Excess pressure field of a mesohigh obtained by subtracting the undisturbed pressure. From Fujita (1959) Precipitation and cold air production in mesoscale thunderstorm systems. *J. Meteor.*, 16, 454-466.

4. MESOCYCLONE AND TORNADO

Early in the 1950s, intersections of pressure-jump lines were regarded as the most likely locations of tornado formation. However, the continued mesoanalysis of the pressure-jump network data revealed repeatedly the existence of mesoscale cyclones in advance of tornadoes (Fig. 6). After the term "mesocyclone" was first introduced in the MESOANALYSIS paper, meteorologists began questioning the feature of the parent cloud of mesocyclone or mesocyclone cloud.

During the 1960-61 spring seasons, the National Severe Storms Project (NSSP) at Norman, Oklahoma conducted an extensive cloud-truth experiment making use of DC-6 A and B, B-26, and B-57 based at Will Rogers Field. Fujita and Chester Newton collaborated in the experiment as flight directors.

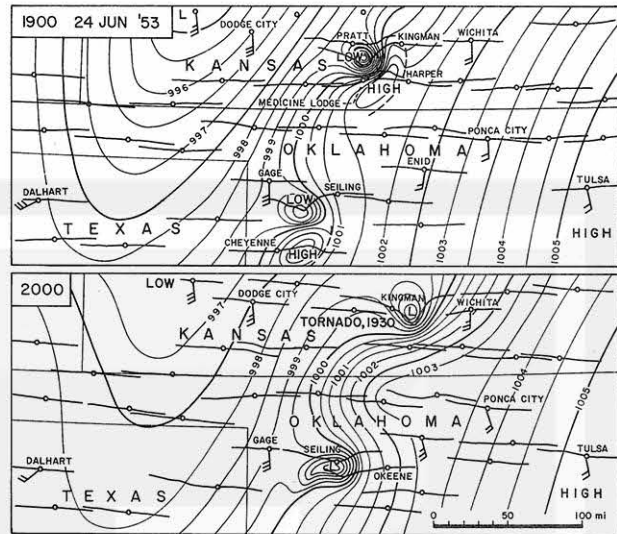


Fig. 6 Mesocyclone, the parent cyclone of tornadoes analyzed by the time-space conversion technique applied to the pressure-jump network data on 24 June 1953. From MESOANALYSIS (1956), Footnote 2.

After exhaustive flights, we found on 21 April 1960 an isolated rotating thunderstorm (Fig. 7). The cloud was characterized by an overshooting top directly above a rotating column of suspected updraft. The 6,000-m flight level winds by DC-6B, Fujita on board, was 75 kts and 53 kts on the south and north sides of the rotating core, respectively. The wind-speed difference was 22 kts (Fig. 8). Chester Newton on board the B-26 at 300-m AGL measured 45 kts inflow winds on the south side and calm wind at the northwest edge of the core echo (Fig. 9).

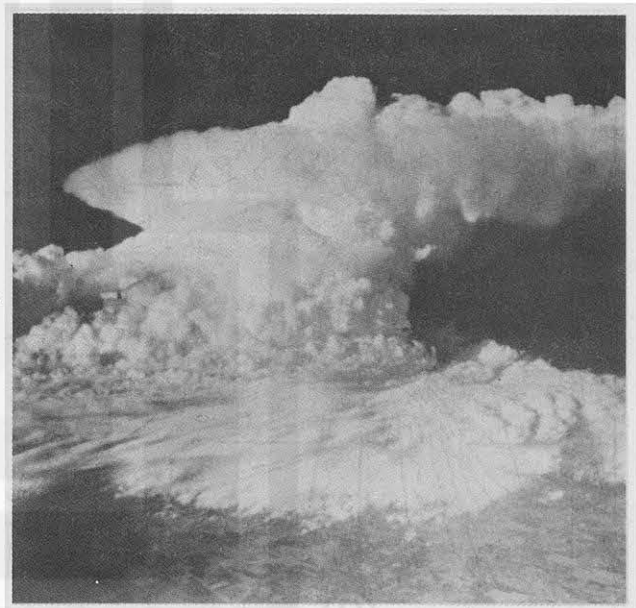


Fig. 7 Aerial photograph of rotating thunderstorm (mesocyclone cloud) of 21 April 1961 taken by Fujita from DC-6B at 1749 CST. From Fujita (1963) Preliminary result of analysis of the cumulonimbus cloud of 21 April 1961. *Mesomet.* Paper 16, U. of Chicago, 16 pp.

It was confirmed, thereafter, that the Kincaid-Selma, Kansas tornado was on the ground between 6:00 and 6:05 p.m., some 15 min after the cloud picture (Fig. 7) was taken at 5:49 p.m. Although the data density and time/space coverage was insufficient, this evidence provided us with the importance of mesocyclones as the parent cloud of violent tornadoes.

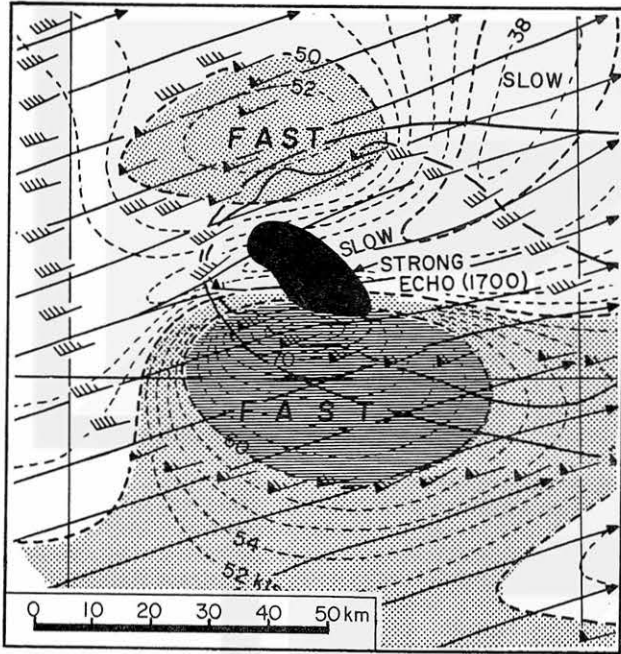


Fig. 8 Composite wind field at 500 mb measured by DC-6B while flying around the cloud in Fig. 7. Same reference of Fig. 7.

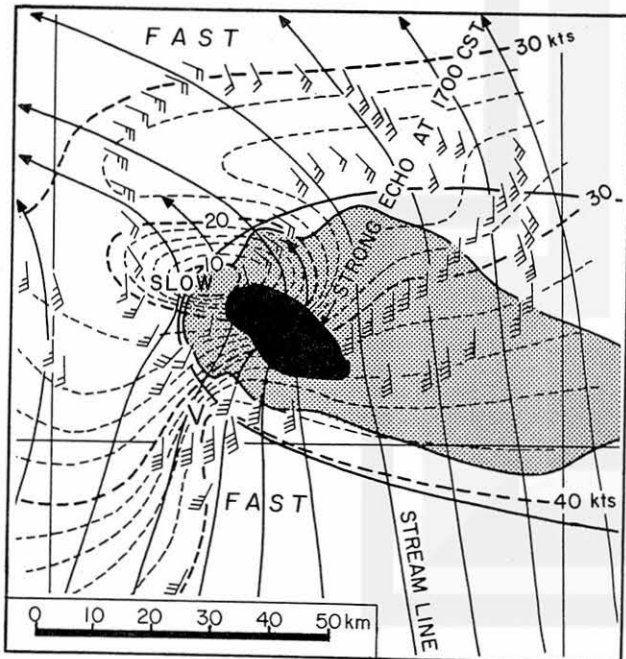


Fig. 9 Composite winds at 300-m AGL measured by B-26 directed by Chester Newton who experienced the worst turbulence ever. Same reference of Fig. 7.

During the 1970s, after investigating in depth the tornadic thunderstorms of 2 June 1971 and the Union City, Oklahoma Tornado of 24 May 1973, the National Severe Storms Laboratory (NSSL) began detecting systematically Doppler-radar signatures of mesocyclones as well as that of tornado vortices (TVS). By 1977, it became evident that the Doppler velocity fields of mesocyclones are recognizable long before the onset of damaging tornadoes. This convincing evidence led to the design of the operational NEXRAD system which will cover the storm-affected regions of the United States.

There is no question that NEXRAD will provide effective means of detecting mesocyclone/tornado vortices, contributing to the improvement of the warning lead time to more than 20 minutes. Nonetheless, the successful use of NEXRAD in mesoscale prediction of severe local storms in various parts of the United States will require both intensive training and operational tests. To achieve the goal, it is important to conduct, after major storms, verification surveys in relating Doppler-velocity fields with near-ground damaging winds. It should be noted also that the storm-bearing velocity fields, both intensity and pattern, could vary with forecast regions as well as the seasons of the year.

5. STATISTICAL PREDICTION OF TORNADES

The occurrence of mesoscale storms at a given location is relatively rare, necessitating long-term statistics of specific storms. Tornado data, for example, are updated in the University of Chicago Tornado Tape for the 74-year period, 1916 - 1989. A total of 34,093 tornadoes are included, allowing us to generate monthly distributions.

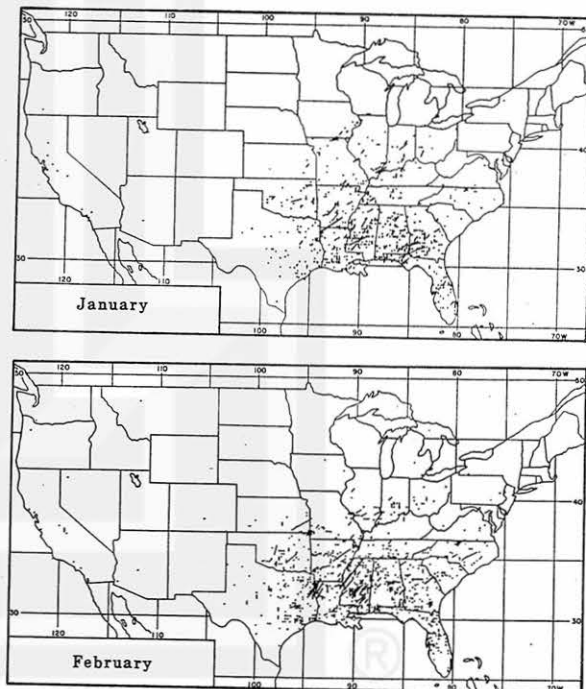


Fig. 10 Tornado distribution of the United States by month. 74 years of tornado data were used. In January and February, tornadoes are centered in the Gulf States. From the University of Chicago Tornado Tape.

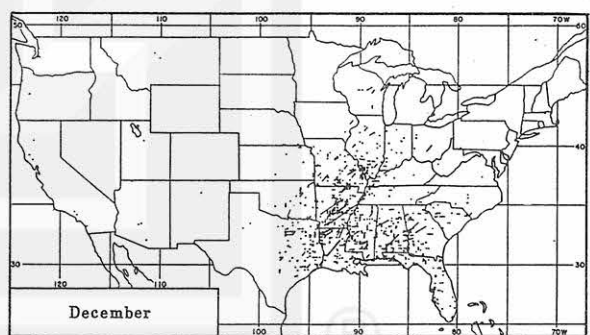
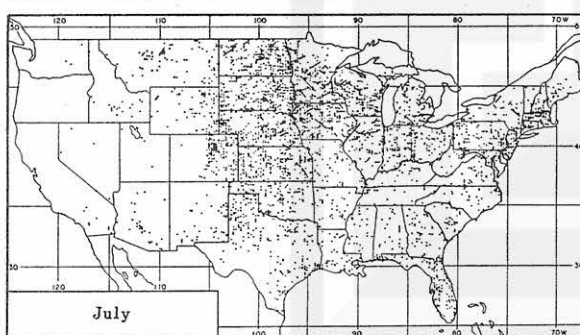
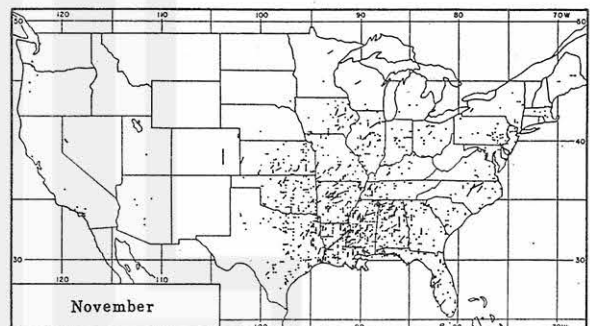
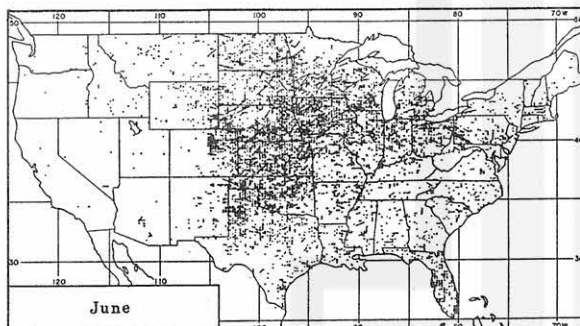
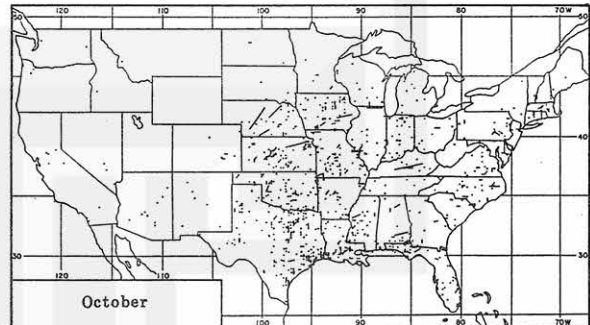
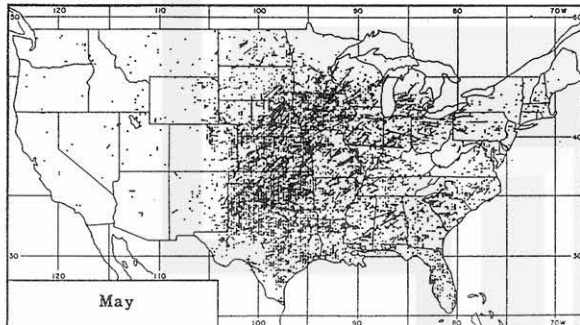
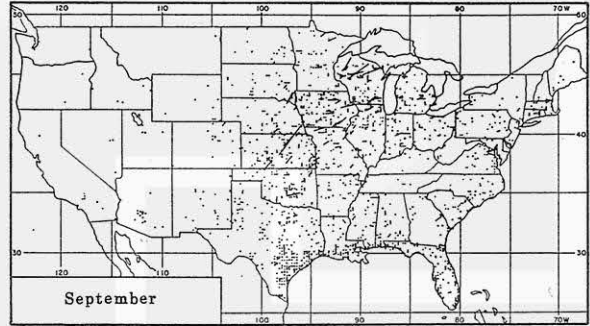
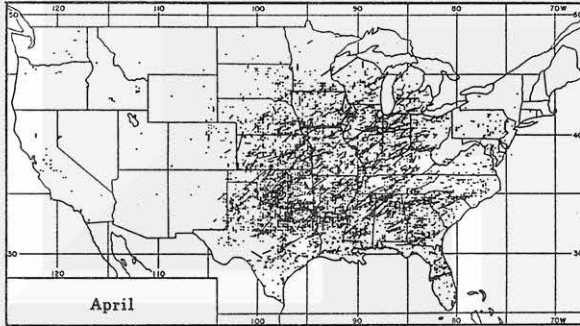
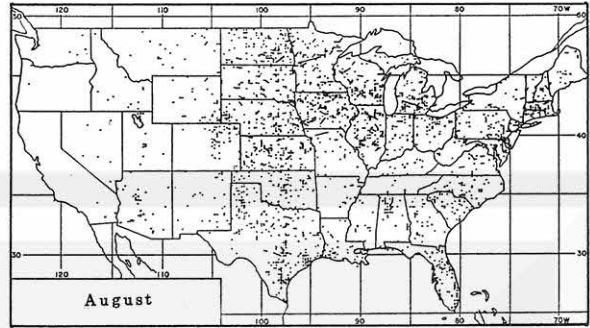
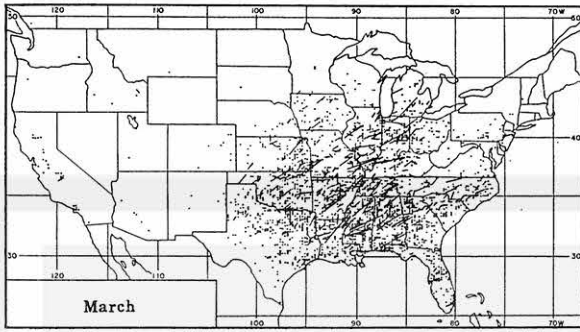


Fig. 10 (continued) Monthly distribution of U.S. tornadoes. Original maps were separated by intensities, F0+F1 (blue), F2+F3 (orange), and F4+F5 (red). After the peak tornado month of April, the northwest boundary of Bermuda High

pushes tornado activities toward the northwest, thinning out the activity in southern states. In November and December, the activity center moves down toward the Gulf States.

Tornado maps by month (Fig. 10) reveal that their climatological distribution is highly seasonal and regional. As has been known, western states rarely experience tornadoes in any season of the year, while early tornadoes in January and February occur frequently in the Mississippi Valley states. Tornadoes spread quickly toward Lake Michigan in March while undergoing an expansion into northern Texas and Oklahoma during the month of April, the peak tornado month in the United States.

Apparently, tornado activities are less significant inside the climatological boundary of the Bermuda High. In May, its northwest boundary becomes identifiable as a zone of tornado-density gradient extending from Lake Ontario to the Ohio River valley. This boundary, becoming more pronounced in June, extends farther to southeast Oklahoma and central Texas. After advancing northward in July, the boundary becomes stationary in August and September. Along with hurricane activities, hurricane-tornadoes spread along the Gulf Coast in September and October. Thereafter, the activity center moves back to the Mississippi Valley states before repeating the climatological annual movement.

The Plainfield Tornado of 28 August 1990 occurred in the southwest suburb of Chicago. The climatological maps of August and September show that a crescent-shaped area of tornado activities extends from Oklahoma, Kansas, Iowa, Wisconsin/Illinois border to southern Michigan. Although the occurrence density is rather low, it is worthwhile to recognize the existence of the crescent-shaped area. It should be noted that climatological distributions cannot be used for day-to-day predictions. These distributions, nonetheless, are useful in recognizing if a specific forecast region is in either high- or low-risk area.

6. SATELLITE IMAGERY

Unlike Doppler radars, current sensors of operational satellites do not penetrate the convectively active region of mesoscale storms which are almost always topped by thick anvil clouds. In spite of handicapped observations, limited only to the detection of cloud-top features, satellite imagery provides us with the global coverage without being affected by either mountain or ocean.

In order to infer the storm activity submerged beneath the anvil surface, it is necessary to detect the anvil-top feature in both visible and infrared imagery first and to determine the most probable processes which give rise to the formation of the specific feature. Of a large number of features determined from operational satellites, the following parameters have been depicted and studied by various authors.

- Areas (pixel counts) of coldest anvil-top temperature and its growth rate.
- Expansion rate of the anvil boundary defined by the visible edge and/or the isoline of a specific temperature.
- Stereoscopic heights of the anvil-top surface determined by dual satellite imagery.
- Warm wake (V-wake) of infrared temperature inside the anvil cloud located in the wake of convective areas.
- Splash out of the anvil material caused by a fast-sinking overshooting top.

● Front-like airflow atop the anvil surface made visible by the mass of cirrus located above the anvil surface. This was confirmed from high-flying aircraft, but not yet from satellite.

Stereoscopic heights have not been used operationally because their computations require dual geostationary satellites with synchronized scans. The polar orbiter with 1-km resolution of infrared sensor can be used in obtaining the high-resolution isotherms of overshooting tops. An example of the Plainfield thunderstorm of 28 August 1990 (Fig. 11) reveals the existence of twin cold tops which induced downbursts prior to the Plainfield Tornado.

An RHI scan of these tops by the United Airlines radar depicted the West Peak at its tallest-echo stage and the East Peak at sinking stage with high-reflectivity core already on the ground. A downburst started beneath the East Peak. This example shows that cloud-top isotherms with 1-km resolution are capable of depicting individual overshooting tops.

Since Mills and Astling³ in 1977 called the warm area on anvil the "warm spot," numerous storm forecasters and researchers attempted to relate severe

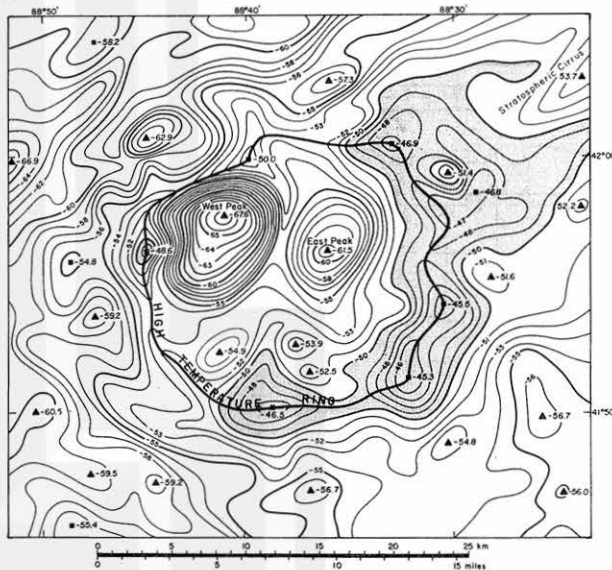
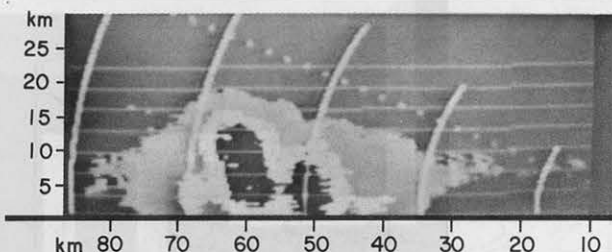


Fig. 11 A detailed isotherm map of the Plainfield thunderstorm of 28 August 1990. Time of the map is 1948 GMT, 30 min before the touchdown time of the major Plainfield Tornado. Two cold peaks are surrounded by a ring of warm, cloud-top temperature, the "High Temperature Ring."

Footnote 3. Mills, P. B., and E. G. Astling (1977) Detection of tropopause penetrations by intense convection with GOES enhanced infrared imagery. Preprints, Tenth Conference on Severe Local Storms, Omaha, Amer. Meteor. Soc., 61-64.

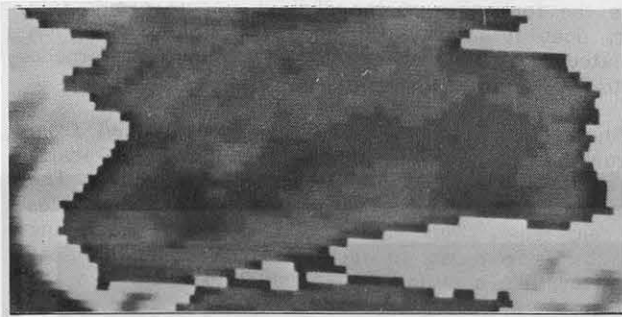


Fig. 12 Infrared imagery of a thunderstorm complex north of Grand Island, Nebraska at 1845 CST 3 June 1980, the day of the Grand Island tornado. Based on the evidence that the warm area extends over 200 km, downwind from the overshooting area to the downwind edge of the anvil, it is assumed that the warming was caused by the stratospheric cirrus drifting away from the source region.

storms with the warm spot which was also called "warm wake," "V-shaped warming," etc. by others.

Although the explanations of the warm wake vary with researchers, most NASA researchers have been relating the warming with high emissivity of the overshooting top. Whereas, Fujita attempted to explain the warming by the warm cirrus in the lowermost stratosphere above the anvil cloud. No matter which hypothesis one might use, the warm wakes are related to the overshooting activities beneath the anvil cloud (Fig. 12).

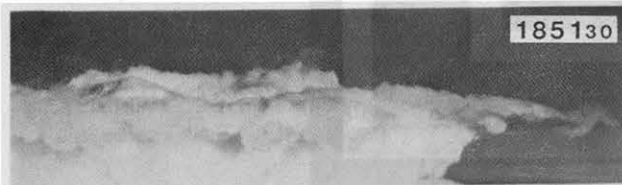


Fig. 13 The splash-out phenomenon photographed from Lear Jet flying over Texas at 12 km MSL. Pictures show the outward escape of anvil materials when an overshooting top sinks rapidly. Photo by Fujita on 6 May 1973. Same reference of Fig. 15.

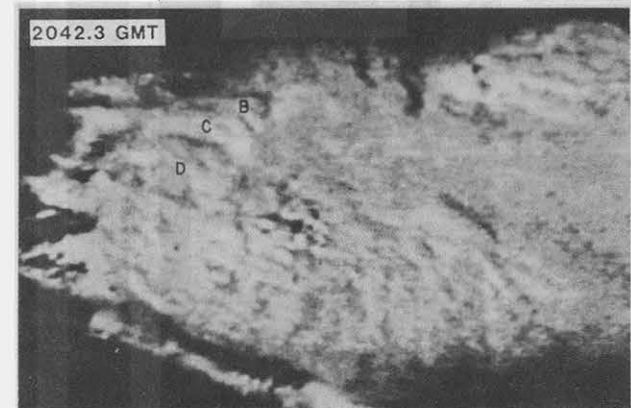
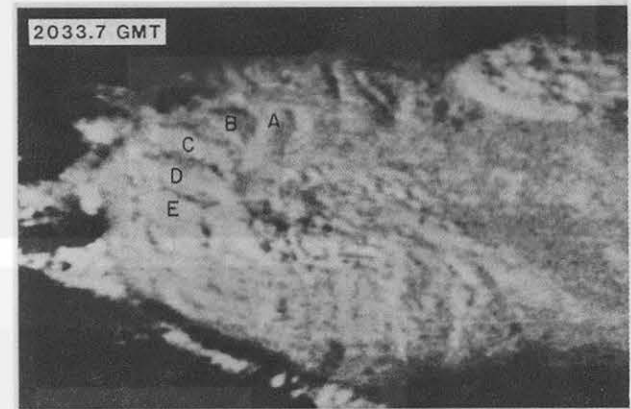
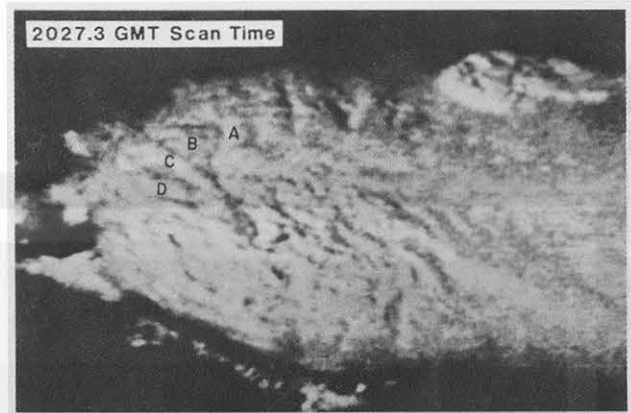


Fig. 14 Anvil-top fingers A through D observed when the Plainfield Tornado was at its peak intensity between 2028 and 2036 GMT 28 August 1990. The pattern of the fingers was most significant at 2033.7 GMT picture time.

It is rather odd to observe the upwind growth of an anvil cloud in strong westerlies. Four pictures in Fig. 13 show the collapsing motion of an overshooting top, acting like a huge rock thrown into a pond at the anvil top. It is seen that anvil-top materials, consisting mostly of ice crystals, splash out in all directions while 51 m/s winds at anvil height were measured at rawin stations.

This splash-out phenomenon was not regarded seriously until after examining the enhanced photos of the Plainfield Tornado cloud (Fig. 14) which displayed five finger-like, splash-out features when it reached the F4 to F5 intensity.

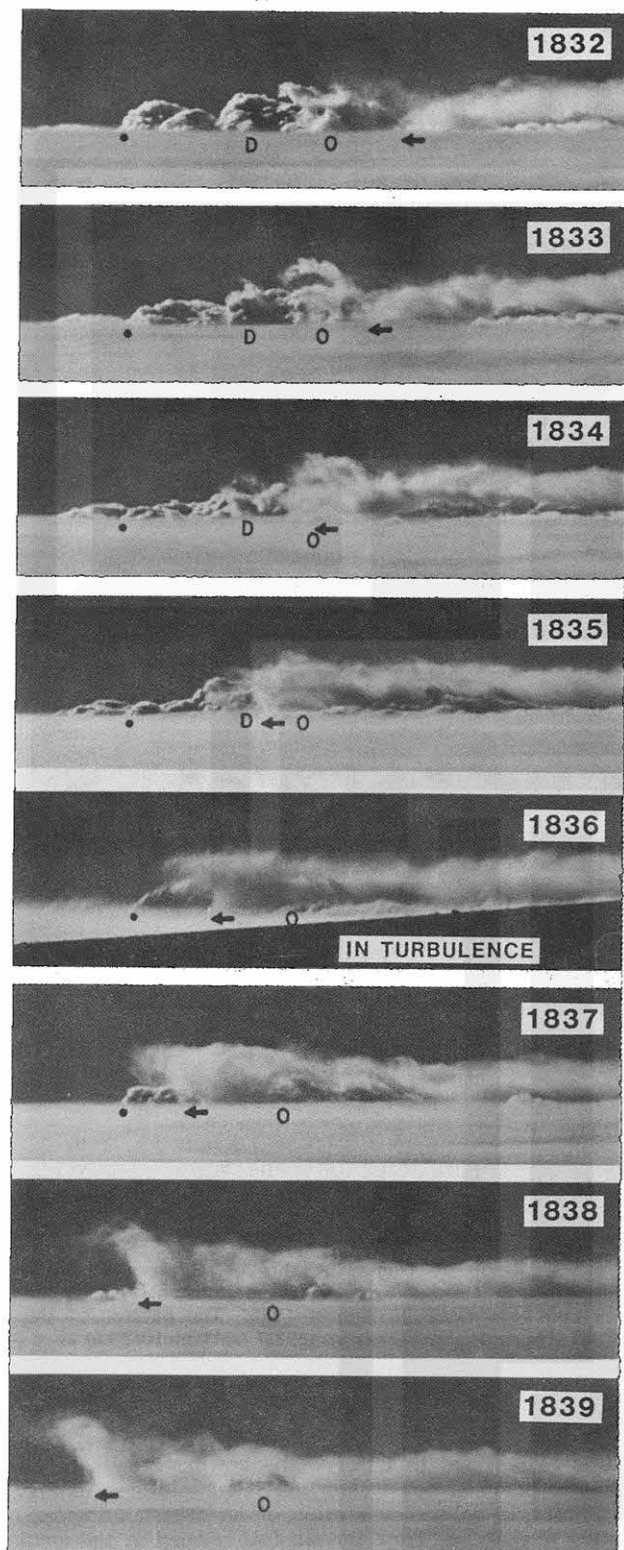


Fig. 15 An anvil-top cold front made visible by a massive movement of the stratospheric cirrus cloud over the anvil surface. These photos, looking north, were taken on 13 May 1972 from Lear Jet at 50,000 ft over Texas. The cirrus was moving west toward the upwind edge of the anvil. From Fujita (1974) Overshooting thunderhead observed from ATS and Lear Jet. SMRP Paper 117, U. of Chicago, 29 pp.

Is the formation of the distinct fingers accidental? Or, does it indicate the collapsing/splashing action related to the intensification of the Plainfield Tornado into F5?

Another interesting phenomenon photographed from Lear Jet is a massive cirrus cloud moving violently over the anvil surface of a hailcloud (Fig. 15). The airflow made visible by the motion of cirrus resembles a cold front. This anvil-top cold front is traveling at 23 m/s from east to west characterized by turbulent motions, like a prominence rising 2 to 3 km into the stratosphere.

It is likely that the source of the cold air is the cold surface of the large anvil lifted by mesoscale convections. The whole anvil surface, acting as a miniature Antarctica, could create katabatic winds strong enough to blow out violently. Because the anvil-top airflow appears to be extremely turbulent, aircraft should avoid such an anvil top.

7. PREDICTION FOR AVIATION AND SPACE

The history of downburst identification dates back to March 1976, eight months after the JFK, New York accident of Eastern 66, when Fujita⁴ proposed the new type of windshear as a probable cause of the accident. It is of historical interest to recall that the concept was received favorably by airlines while most meteorologists expressed their opposing views at that time.

After the opinion poll in the 17 March 1979 issue of Science News, the meteorological community gradually became supportive of the downburst because more people began looking for the downburst phenomena, obtaining cloud pictures (Fig. 16).

Three fact-finding experiments; NIMROD 1978, JAWS 1982, and MIST 1986, conducted jointly by the National Center for Atmospheric Research (NCAR), the Univer-

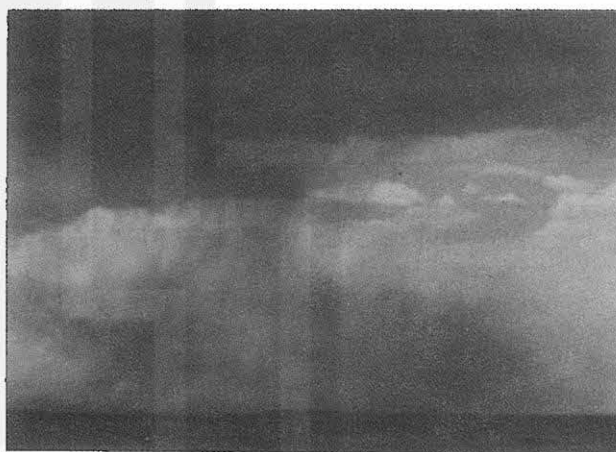


Fig. 16 A Colorado microburst of 27 July 1978 at 2:30 p.m. MDT photographed by Fujita in Cliff Murino's car on the way to the Grover research site.

Footnote 4. Fujita, T. T. (1976) Spearhead echo and downburst near the approach end of a John F. Kennedy airport runway, New York City. SMRP Res. Paper 137, Univ. of Chicago, 51 pp.

sity of Chicago, and MIT Lincoln Laboratory documented successfully the existence of dry and wet microbursts in various parts of the United States. These observational results accelerated the termination of the "downburst controversy" which started in 1976.

Needless to say, NCAR played the important role in the fact-finding experiments of microbursts in various stages of data collection and research. It is now expected that Terminal Doppler Radars are deployed at major U.S. airports in coming years. Like any other detection method, we will have to cut down false alarm rates while issuing the true alarms, the tone of which will vary with the intensity of windshear. Because the pilot makes the final decision, it would be necessary to give him all possible informations in usable forms. These informations are obtained by

Ground sensors: Terminal Doppler Radar, the major contributor; Low Altitude Windshear Alert System (LLWAS), the complementary system; airport anemometer for non-LLWAS airports

Airborne sensors: Airspeed-groundspeed difference; vector change of wind at aircraft; 3-axis accelerometer; airborne radar; infrared detector

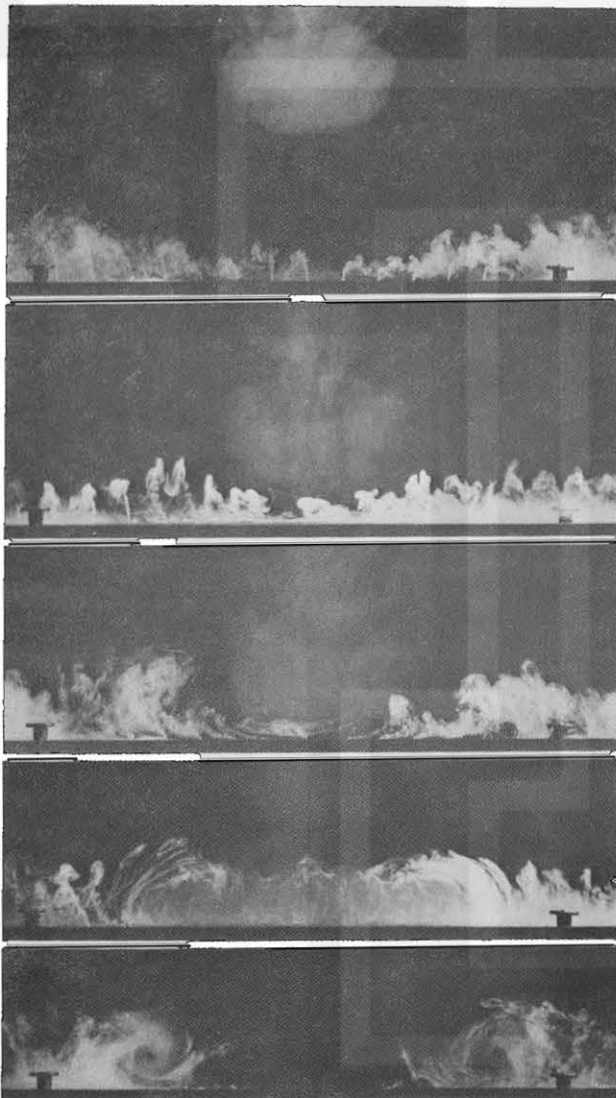


Fig. 17 Five stages showing the evolution of a laboratory microburst generated in the Fujita Laboratory, University of Chicago.

Human sensor: Monitoring accelerations, cloud base and rainshaft, dust clouds on the ground; pilot reports; microburst statistics by time of day and season of the year; basic knowledge of microburst avoidance.

A laboratory experiment (Fig. 17) shows that a microburst is a transient phenomenon, completing its evolution very fast. Five stages of the evolution are — descending, pre-contact, contact, curling-up, and ring-vortex stages. In the laboratory a microburst ends within five seconds after touchdown.

Mesoscale prediction for space activities could be more critical than aviation, especially when shuttle flights are involved. The prediction must include vertical distribution of wind and windshear, cloud types, cover and trend, air-temperature, lightning and precipitation, and the crosswind at the runway for emergency landing, when required. Furthermore, the prediction must be specific and accurate.

For instance, the liftoff of Shuttle Atlantis in August 1991 was an interesting case to remember. Initially its launch had been postponed for about two weeks to 1 August when a large number of weather researchers working for the CAPE Experiment gathered at the NASA viewing site. In spite of a long wait and expectation, the launch was cancelled because of the weather. Next morning, cumulus activities subsided and the shuttle landing crosswind weakened as predicted. A spectacular launch took place at 1102 EDT 2 August, precisely on schedule.

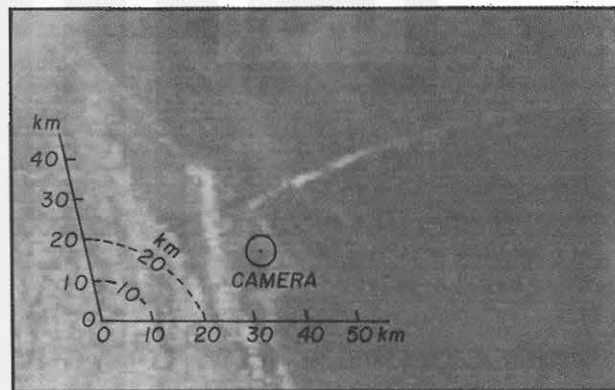


Fig. 18 The plume left behind by Shuttle Atlantis. Photo by GOES 7 scanned at 1105 EDT, 3 min after the liftoff from launch pad 39A at the Kennedy Space Center, Florida.

The plume of Atlantis was photographed by GOES at 1105 EDT, 3 minutes after the launch. Seen in the picture (Fig. 18) is a thin, long plume extending east-northeast from the launch pad into the Atlantic.

In an attempt to determine the motion of the plume embedded inside the atmosphere, Fujita and his associates monitored the plume with a whole-sky camera placed 11.8 km south of the launch pad. Pictures taken at 2.5 min intervals recorded the plume changes during the 60-min period following the launch.

At 1105 EDT, the plume was a curved line beginning to show a leftward displacement at the jet-stream height 8 to 13 km MSL. Five min later at 1110 EDT,

the plume at jet level was pushed farther, resulting in a significant distortion. Meanwhile, the plume at 14 km MSL turned into a lump 3 km in diameter. The plume at the jet level began forming double Vs at 1132 EDT, suggesting the existence of double maxima at two different heights. At the same time, the lump inside the lowermost stratosphere turned into a vortex 4 km in diameter (Fig. 19).

This photographic evidence indicates that a plume such as this can be used in hindcasting the mesoscale weather events which had taken place after individual launches.

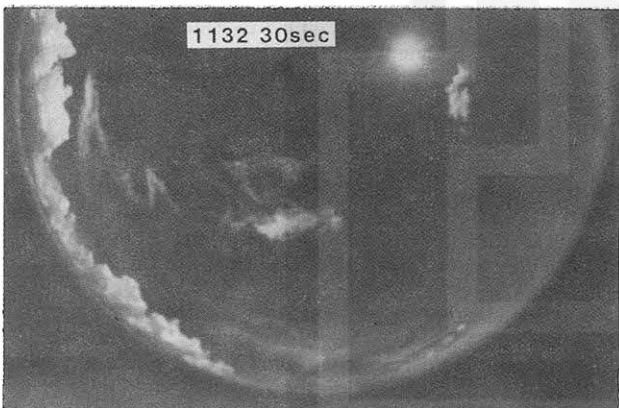
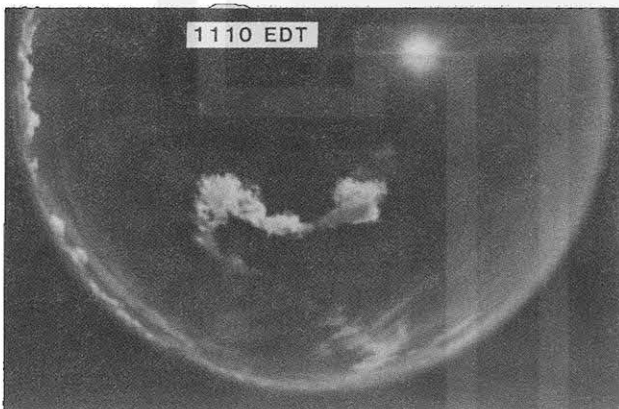
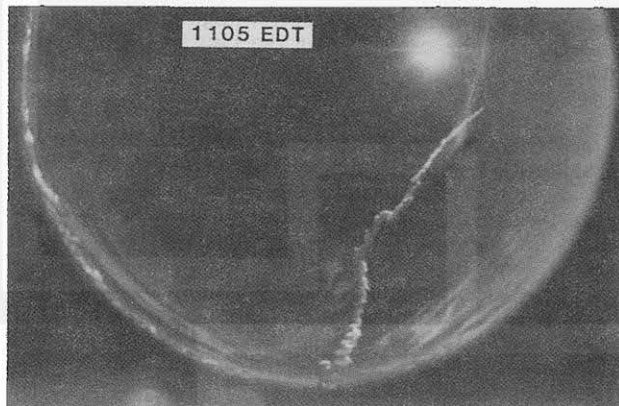


Fig. 19 Three whole-sky photos selected from the 2.5 min sequence taken between launch time and local noon. During the one hour period, the plume was distorted by the weak easterly jet which generated double Vs drifting westward.

Acknowledgements

The basic research leading to this overview paper was performed both in Japan and in the United States between 1948 and 1991. The initial research in 1948-53 was done at the Kyushu Institute of Technology under grants from the Science Research Foundation of Japan, while the extensive mesometeorological research in 1953-90 was sponsored by NSF, NASA, NOAA/ NESDIS and other U.S. Government Agencies.

The overview of the author's research results, both published and unpublished, was supported by NOAA/ NESDIS under Grant NA16EC0425-01, by NSF/UCAR under Grant S9129, and in part by NASA under Grant NAG8-886.